ISBN: 978-3-95450-231-8 ISSN: 2673-5490 doi: 10.18429/JACoW-IPAC2023-WEPL011

COMMISSIONING OF ORBIT FEEDFORWARD SYSTEM FOR HEX SUPERCONDUCTING WIGGLER AT NSLS-II*

Y. Hidaka†, Y. Li, T. Tanabe, Y. Tian, G. Wang
Brookhaven National Laboratory, Upton, New York, USA

Abstract

A 1.2-m-long superconducting wiggler with the peak field of 4.3 T and period length of 70 mm has been recently installed for the High energy Engineering X-ray (HEX) Diffraction beamline at Cell 27 of NSLS-II Storage Ring. The commissioning result for the orbit feedforward system will be presented, including the residual dispersive pattern in horizontal orbit after correction and non-negligible hysteresis effects. The impact of large residual field integrals on the active interlock envelope will be also discussed.

INTRODUCTION

A 1.2-m-long superconducting wiggler (SCW) with 4.3-T peak field [1] has been recently installed in the NSLS-II storage ring at Cell 27 for the High energy Engineering X-ray (HEX) beamline and successfully commissioned with electron beam. This device has residual field integrals that vary with the magnetic field strength, controlled by its main coil current, but the variation is particularly large. Hence it requires orbit correction whenever the main coil current changes to minimize global orbit distortion. This correction is automatically performed by an orbit feedforward system implemented via EPICS [2], as with any other insertion devices (IDs) installed at NSLS-II. This paper presents the measurements of residual field integrals for the SCW and the effectiveness of the orbit feedforward system to compensate them.

ORBIT FEEDFORWARD CORRECTION SCHEME

When there is no ID in a straight section, beam propagates through the region without any deflection. If an ID is present, a beam goes through the device, experiencing potentially multiple kicks in both x and y planes due to residual field integrals, with the beam coming out at an angle and/or an offset, as shown in Fig. 1. The first field integrals I_{1x} and I_{1y} are responsible for the non-zero exit angle, whereas the second field integrals I_{2x} and I_{2y} lead to non-zero exit offset. No matter how complicated the beam trajectory within the ID is, how the global orbit will be distorted is determined only by the exit angle and offset values.

Because of this, for the purpose of orbit distortion correction due to the residual field integrals, the ID of length L could be modelled simply as a drift of length L with an upstream (US) and a downstream (DS) kick in a lattice simulation, as illustrated in Fig. 1. The relationships between the 1st and 2nd field integrals (I_1 & I_2) and the US and DS virtual kicks (θ_{US} & θ_{DS}) are the following:

$$I_1 = B\rho(\theta_{\mathrm{US}} + \theta_{\mathrm{DS}}), \quad (1)$$

$$I_2 = B\rho \cdot L\theta_{\mathrm{US}}, \quad (2)$$

where $B\rho$ is the magnetic rigidity and ~10 T · m for the beam energy of 3 GeV at NSLS-II.

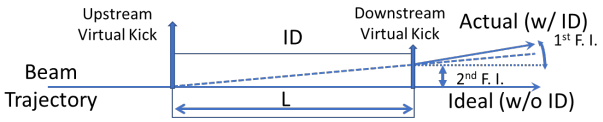

Figure 1: Relationship Between Upstream and Downstream Virtual Kicks (θ_{US} and θ_{DS}) and the 1st and 2nd Field Integrals (I_1 and I_2) for an ID with Device Length of L.

A beam-based measurement of residual field integrals for an ID like in-vacuum undulators (IVUs) and elliptically polarizing undulators (EPUs) consists of measuring the beam orbit with the ID at a reference state (typically chosen to be the state with its gap fully open) and the beam orbit at another state with a different gap (and phase for EPUs). In a simulation, the two virtual kick angles are adjusted until the simulated closed orbit distortion fits well with the difference orbit between the two measured orbits. Then we can estimate the field integrals using Eqs. (1) and (2).

Incidentally, if the locations of the virtual kicks coincide with those of the orbit correction magnets dedicated for compensating the field integral change, the orbit error can be completely cancelled by adjusting the corrector magnet strengths to generate kicks with the same magnitudes as the virtual kicks, but with opposite signs.

If this is not the case, an orbit response matrix (either design or measured) for the dedicated correctors can be used to correct the orbit error iteratively. A lookup table with respect to the ID gap (and phase for EPUs) can be then created by collecting the values of corrector setpoints that cancel the orbit distortion. For the SCW, the main coil current (I_{main}) is varied, instead of gap.

The orbit feedforward program for the SCW continuously monitors the I_{main} readback value and adjusts the power supply current setpoint values of the corrector magnets according to the lookup table with linear interpolation.

BEAM-BASED FIELD INTEGRAL MEASUREMENT RESULTS

For the SCW field integral measurements using beam orbit, the ID state with the maximum main coil current (I_{max}) of 440.5 A was selected as the reference state, instead of the off state (i.e., 0 A), equivalent to the fully open state for an IVU. This choice was made to avoid non-reproducible reference orbits arising from hysteresis. This is why the

* Work supported by U.S. DOE under Contract No. DE-SC0012704.
† yhidaka@bnl.gov

ISBN: 978-3-95450-231-8 ISSN: 2673-5490 doi: 10.18429/JACoW-IPAC2023-WEPL011

estimated virtual kick angles at I_{max} are zero, while those values are non-zero at 0 A in Fig. 2.

The hysteresis effect is evident in Fig. 2. The measurements for the upramp were taken by varying I_{main} from 0 to I_{max} with the step size of 10 A, after a few full cycles between 0 and I_{max}. The down-ramp measurements were performed when I_{main} was lowered from I_{max} to 0. If there is no hysteresis, the upramp and downramp curves should agree well, but they differ by more than 100 μrad horizontally around $I_{main} \approx 40$ A.

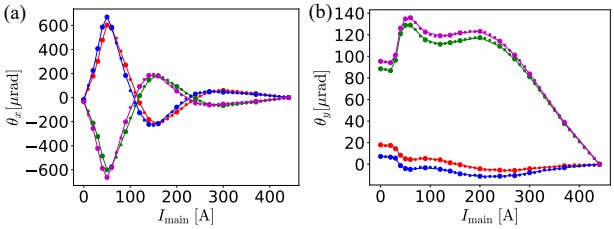

Figure 2: Estimated Virtual Kick Angles from Measured Orbit Differences vs. I_{main}, Which was Varied From 0 to 440.5 A with 10-A Steps for Upramp Cycle (red/green for US/DS), While the Current Change was Opposite for Downramp Cycle (blue/magenta for US/DS).

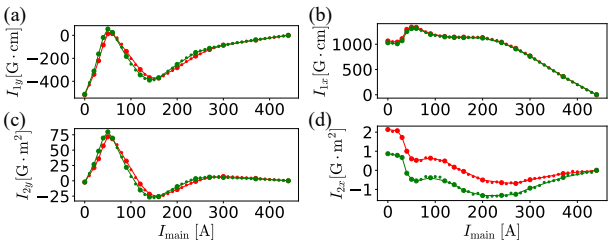

Figure 3: Estimated (a) I_{1y}, (b) I_{1x}, (c) I_{2y}, and (d) I_{2x} vs. I_{main}, by Converting the Estimated Virtual Kick Angles Shown in Fig. 2 with Eqs. (1) and (2). Red and Green Lines Correspond to Upramp and Downramp, respectively.

Figure 3 shows the corresponding estimated residual 1st and 2nd field integral values, based on the virtual kick angle estimates shown in Fig. 2, using Eqs. (1) and (2). This SCW has the largest residual field integrals measured at NSLS-II so far.

ORBIT FEEDFORWARD PERFORMANCE

An orbit response matrix (ORM) was measured with $I_{main} = 440.5$ A for six orbit correction coil channels dedicated for the SCW right at the ends of the device as well as the two nearby ring correctors. One Helmholtz coil and two auxiliary (AUX) coils are installed on the US side, and the same is true for the DS side. All of these coils can only correct orbit horizontally. For the vertical orbit correction, we are using the two ring correctors for now.

The response of the US AUX coils was only 12% of that of the US Helmholtz coil, while the response of the DS AUX coils was only 6% of that of the DS Helmholtz coil. Besides, the AUX coils are very close physically to the Helmholtz coils, resulting in sizable degeneracy. Hence, we decided to only use the US and DS Helmholtz coils for horizontal correction.

For construction of a feedforward table, we manually selected 16 I_{main} setpoint values (unequally spaced) that can effectively trace the highly nonlinear field integral curves (Fig. 3) with simple linear interpolation. Using the measured ORM, the global orbit distortion at these setpoints were iteratively corrected as much as possible. The upramp cycle was used for table generation because upramp cycles are much more likely to be encountered during beamline operation. The resulting table values are plotted in Fig. 4, which are quite similar in shape to Fig. 2 for the horizontal plane (Ch. 1 & 2), as expected. On the other hand, the curves for the vertical plane (Ch. 3 & 4) differ since the vertical ring correctors are located very far from the SCW.

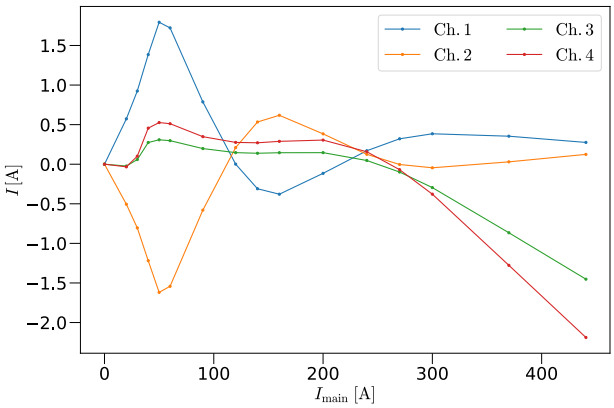

Figure 4: Generated Orbit Feedforward Table for 4 Correction Coil Setpoints (2 horizontal and 2 vertical).

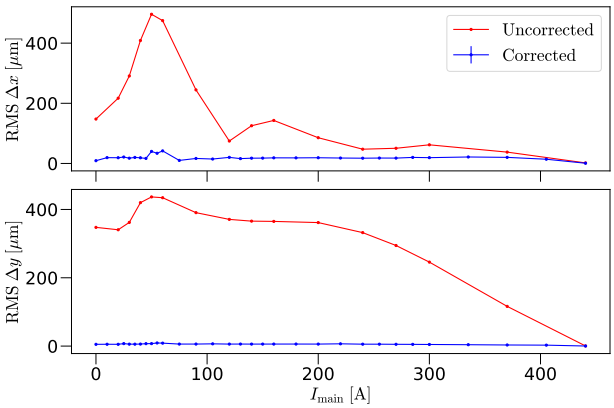

Figure 5: Horizontal (top) and Vertical (bottom) Orbit Distortion RMS Values at all 180 BPMs in the Ring vs. I_{main} with the Feedforward System Turned Off (red) and On (blue).

The effectiveness of the orbit feedforward system with this table is shown in Fig. 5. The RMS value of the residual vertical orbit distortion was less than 10 μm for the entire range of I_{main}. The horizontal RMS values were mostly ~20 μm with up to 40 μm around 50 A. This level of correction is not as good, compared to the other existing IDs (typically less than 10 μm). However, the residual distortion is sufficiently small that FOFB [3] and UOFB [4] can maintain

ISBN: 978-3-95450-231-8 ISSN: 2673-5490 doi: 10.18429/JACoW-IPAC2023-WEPL011

excellent short- and long-term orbit stability at all the other beamlines while the SCW is being ramped.

The difference between the orbits with $I_{main} = 0$ and $I_{main} = I_{max}$ with the feedforward system enabled is shown in Fig. 6. The pathlength increase due to large horizontal wiggling motion inside the SCW decreases beam energy. This effect can be observed as the dispersive orbit pattern in the Δx plot. This orbit distortion cannot be corrected with the feedforward system, but can be compensated with the RF frequency feedback feature integrated in UOFB [4].

The Δy plot in Fig. 6 shows large vertical residual errors at the two BPMs at $s \sim 700$ m. These BPMs are located between the SCW and the ring correctors used for vertical orbit correction. The orbit feedforward system can only minimize the orbit distortion at BPMs outside of the straight section where the SCW is installed. Other operational issues related to the use of the ring correctors will be discussed in the next section.

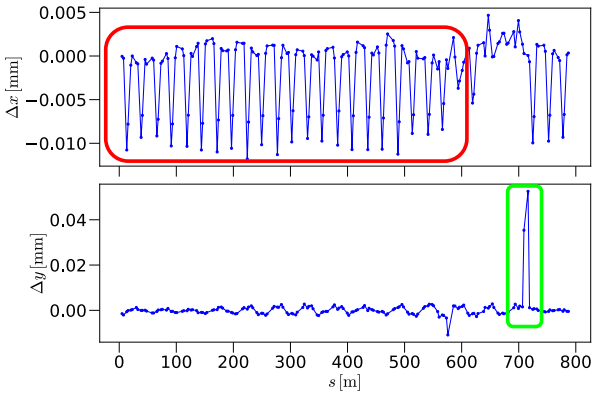

Figure 6: Difference Orbit at $I_{main} = I_{max}$ A with respect to Orbit at $I_{main} = 0$. Dispersive Pattern Due to Pathlength Change is Visible Horizontally (red box), While Large Vertical Distortion Is Left At A Few BPMs (green box) Due To The Correction Coils Being Located Far From The SCW.

OPERATIONAL ISSUES DUE TO USE OF REMOTE CORRECTION COILS

One issue caused by the use of the vertical correctors being far from the kick source (i.e., the SCW) is the potentially large error in estimating the angle and offset value of the beam trajectory within the SCW, as illustrated in Fig. 7, showing the case for $I_{main} = 30$ A. For the given virtual kicks (green arrows) at the SCW (green box), the kick angles of the vertical ring correctors (blue arrows) are adjusted by the feedforward system to minimize global orbit distortion. The beam angle and offset at the center of SCW are estimated to be -18.6 μrad and -129.0 μm from the position readings at BPMs P7 and P8, assuming the straight-line trajectory (black solid line). However, the actual angle and offset, represented by the red dash-dot line, are -21.8 μrad and -179.1 μm. The estimation errors for the angle and offset are summarized for the entire range of I_{main} in Fig. 8. In the worst case, the angle and offset could be off by 18 μrad and 60 μm, respectively. These errors would not occur if dedicated correction coils were located near the SCW. Our active interlock (AI) system dumps beam for equipment protection if it detects the beam angle or offset of any ID deviates from the center by more than 250 μrad and 500 μm. Hence, the permissible AI envelope needs to shrink by the amount of these errors to be conservative.

Another issue is the large ID BPM beam-based alignment (BBA) deviation at P7 and P8. This special real-time diagnostic measurement value tells us unexpected BPM physical/electronic movements as well as angle changes for all kicks within the bounding BPMs (i.e., P6 and P1 in Fig. 7) [5, 6]. The large kick angle changes with variation of I_{main} resulted in the deviation of 150 μm vertically P8 at a fixed ring beam current. As an administrative policy, we are required to investigate the cause for any ID BPM BBA deviation above 100 μm. Because of this, the HEX beamline is currently restricted to operate at $I_{main} \leq 300$ A.

Due to these problems, we are planning to convert two unused horizontal AUX channels to vertical ones in the near future. Then we will no longer need to use the ring correctors, and the large vertical kicks can be compensated very close to both ends of the SCW.

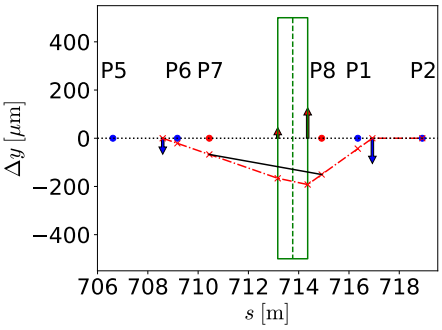

Figure 7: Large Virtual Kicks (green arrows) And the Vertical Corrector Kicks (blue arrows) Located Far from SCW (green box) Lead to Large Errors in Estimating Beam Angle and Offset At SCW. P1 Through P8 Are BPM.

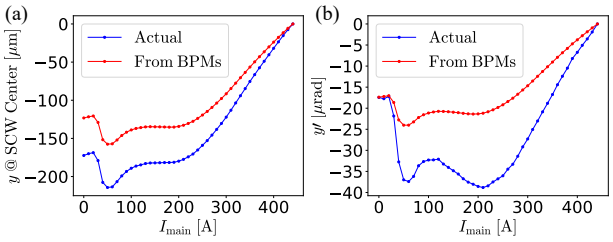

Figure 8: Estimation Errors for Vertical (a) Offset at the Center of SCW and (b) Angle vs. I_{main}.

CONCLUSION

We have successfully commissioned a newly installed SCW at Cell 27 of NSLS-II Storage Ring. The orbit feedforward system has been successfully implemented and validated to suppress most of the residual field integrals, which allowed the HEX beamline to start commissioning its beamline components. The problems arising from the fact that correction coils for vertical orbit compensation are not closely located to the SCW were identified and will be remedied shortly with hardware modifications.

ISBN: 978-3-95450-231-8 ISSN: 2673-5490 doi: 10.18429/JACoW-IPAC2023-WEPL011

REFERENCES

[1] T. Tanabe *et al.*, "Construction of Cryogen-Free 4.3T Superconducting Wiggler for NSLS-II Ring", *IEEE Trans. Appl. Supercond.*, vol. 32, no. 6, pp. 1-4, Sep. 2022, Art no. 4102004. doi:10.1109/TASC.2022.3173248.

[2] L. R. Dalesio *et al.*, "EPICS architecture", Los Alamos National Lab., Los Alamos, NM, USA, Rep. LA-UR-91-3543, Jan. 1991.

[3] Y. Tian and L.-H. Yu, "NSLS-II Fast Orbit Feedback with Individual Eigenmode Compensation", in *Proc. PAC'11*, New York, NY, USA, Mar.-Apr. 2011, paper WEODN4, pp. 1488-1490.

[4] Y. Hidaka, Y. Li, R. M. Smith, Y. Tian, G. M. Wang, and X. Yang, "Unified Orbit Feedback at NSLS-II", in *Proc. NA-PAC'22*, Albuquerque, NM, USA, Aug. 2022, pp. 795-798. doi:10.18429/JACoW-NAPAC2022-WEPA71

[5] Y. Hidaka *et al.*, "Investigation on Mysterious Long-Term Orbit Drift at NSLS-II", in *Proc. IPAC'19*, Melbourne, Australia, May 2019, pp. 2728-2731. doi:10.18429/JACoW-IPAC2019-WEPGW102

[6] Y. Hidaka, B. N. Kosciuk, B. Podobedov, J. Rank, and T. Tanabe, "A New Orbit Feedforward Table Generation Method for Insertion Devices", in *Proc. IPAC'19*, Melbourne, Australia, May 2019, pp. 2724-2727. doi:10.18429/JACoW-IPAC2019-WEPGW101